

Volume Title
*ASP Conference Series, Vol. **Volume Number***
Author
 © ***Copyright Year*** *Astronomical Society of the Pacific*

Using Absorptive Linear Polarization Spectroscopy to Understand Imbedded Stars

J. R. Kuhn, B. Geiss, and D. M. Harrington

*Institute for Astronomy, University of Hawaii,
 34 Ohia Ku St, Pukalani, Maui, HI 96790, USA*

Abstract. Sensitive measurements of the linearly polarized spectra of stars can be used to deduce geometric properties of their otherwise unresolved circumstellar environments. This paper describes some of the evidence for optical pumping and absorptive linear polarization and explores some interesting applications of linear spectropolarimetry for obtaining spatial information from imbedded stars.

1. Introduction

Linear spectropolarimetry of stars obtained with polarization sensitivity of 0.1% or better often shows linear polarization variability across absorption lines (cf. Vink et al. 2002, 2005b; Harrington and Kuhn 2007, 2009a,b). This effect is observed over a broad range of stellar conditions and in many lines in a stellar spectrum. We've shown (Kuhn et al. 2007) that the anisotropy of the stellar radiation field can lead to anisotropy in the ground-state atomic energy levels responsible for the observed stellar absorption lines. This quantum mechanical effect is called optical pumping (OP) in the laboratory (Happer 1972), and has been known for some time to yield observable linear polarization effects in the solar spectrum (Trujillo Bueno and Landi Degl'Innocenti 1997). Using detailed radiative models of Hydrogen absorption above the surface of a star we've shown (Kuhn et al. 2007) that H_α is often quite sensitive to optical pumping. Our earlier models didn't include the effects of hyperfine coupling and considered only the low-lying atomic levels in Hydrogen.

Interpreting H_α polarization is complicated by the degenerate hyperfine transitions that are not resolved in typical stellar spectropolarimetry measurements. In this paper we'll outline possibilities for simplifying the interpretation of the observed polarization across stellar absorption lines. For example, from certain non-hydrogenic lines we can show that optical pumping, not scattering polarization, is the mechanism responsible for producing spectropolarimetric variability.

In stellar systems where the lines in the Balmer or Paschen sequence originate from the same circumstellar region, we find further support for the OP model by showing that the linear polarization ratios for the strongest hydrogen lines can be computed from simple models. These polarization ratios may be used to constrain the local circumstellar environment. We examine several stellar systems where optical pumping in the Balmer lines appears to originate from the same region and we speculate on how detailed comparison of optical pumping in different lines can be developed as a useful tool.

In stellar systems with a rotating disk we illustrate how the absorptive linear polarization due to optical pumping can be used to determine some basic geometric properties. Thus, the orientation of a disk in the sky and its tilt with respect to the plane of the sky can be inferred from the absorptive linear polarization line profiles. Finally we show how linear spectropolarimetric data can be inverted to obtain spatially resolved “images” of the intervening gas near the imbedded star.

2. Absorptive Polarization

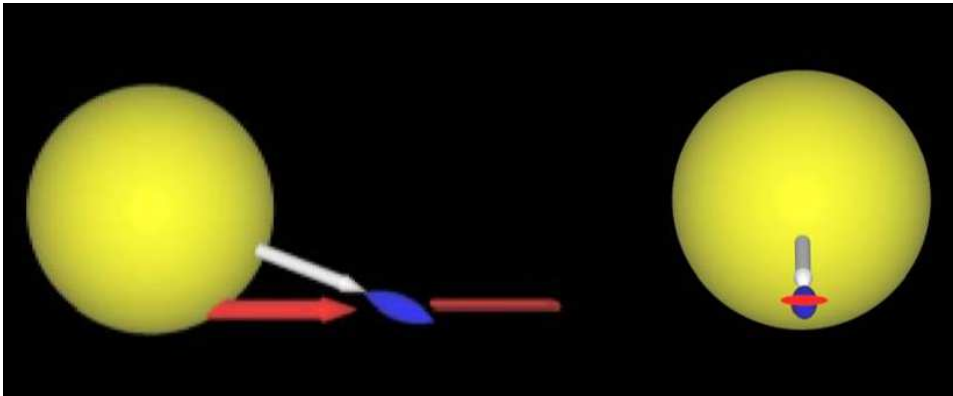


Figure 1. Optical pumping geometry for a cloud (blue ellipse) observed along a line-of-sight (red arrow) and radiatively excited from anisotropic stellar radiation (white arrow)

Optical pumping originates from the lower level of atomic transition levels where the equilibrium density of the magnetic quantum number states depends on the magnetic quantum number m . For example, if a lower-level state with $J=1$ has a different electron density for the $m = 0$, compared to the $m = -1, +1$ levels then these atoms will yield a line opacity which depends on the incident light direction and linear polarization states. The population anisotropy is determined by the angular anisotropy of the incident radiation. The optical pumping (OP) mechanism geometry we describe can be simplified to a “pumping beam (or light cone) represented by the mean direction of the radiation which induces anisotropy in the atomic sublevels, and a “probe” beam which is the direction of the optical radiation that is selectively absorbed by the pumped atomic gas in the line-of-sight to the observer.

Figure 1 shows schematically how OP works in the circumstellar environment of a star. A classical analogy is indicated in this figure. We consider an absorptive “cloud” between the observer and a star indicated by the blue ellipse. The pumping radiation originates along the direction of the white arrow and effectively polarizes the dipole response of the atomic system to lie along this direction, indicated schematically here by the elongated blue ellipse. Light which is absorbed by the cloud originates from the photosphere of the star along the line-of-sight direction to the observer (the red arrow). The absorbed radiation induces an electronic dipole response in the cloud which favors a direction along the elliptical long axis. Thus, for initially unpolarized radiation it is the probe beam electric field direction most closely aligned with the ellipse which is selectively absorbed and scattered. The perpendicular electric field orientation

is transmitted with lower opacity. The red ellipse projected in the side panel shows the enhanced polarization direction of the transmitted light as seen from the observers perspective. In general OP absorptive polarization yields a transmitted beam polarized perpendicular to the plane containing the pumping and probe beam directions, although a negative polarization can be induced in some atomic transitions as we show below.

2.1. Database

Our group has amassed a considerable database of precision linear spectropolarimetry measurements from a broad range (about 100) of “imbedded” stars. This includes HAeBe’s, Post-AGB, RV-Tau’s, Wolf-Rayet, and others (Harrington and Kuhn 2007, 2008, 2009a,b). Part of this database has been obtained with our own HiVIS spectrograph on the Haleakala AEOS 3.7m telescope but it also includes data obtained from the ESPaDOnS instrument on the CFHT. The data described below was obtained with the CFHT and comes primarily from archival data records. These data were obtained with spectral resolution $R > 50000$ and with typical 2σ linear spectropolarimetric accuracy of 0.1% in the line profiles.

2.2. Non-scattering Lines

Various mechanisms have been proposed to describe the linear spectropolarimetric variability seen in stellar absorption lines (cf. Vink et al. 2005; McLean 1979; Oudmaijer and Drew 1999). For example, scattering polarization from free electrons or resonant line scattering is often invoked (McLean 1979). Unpolarized line scattering in combination with polarized Thomson scattering can also yield polarization variability across spectral lines (McLean 1979). Scattering polarization requires an atomic upper level which allows for a population anisotropy. This occurs if the net angular momentum (including nuclear spin coupling) yields a total angular momentum greater than $1/2$. Calcium is relatively abundant with no net nuclear spin. The CaII triplet transitions at 849.8, 854.2, and 866.2nm are an excellent multiplet to test scattering as a polarization mechanism since the lines have similar formation properties and the longest wavelength term cannot be polarized by scattering. Manso Sainz and Trujillo Bueno (2003) studied these transitions in the solar spectrum in order to explain observed solar spectral polarization.

The 866.2nm transition upper level is a $J=1/2$, $^3P_{1/2}$ state, while the other transitions originate from the $^3P_{3/2}$ level. The lower level in each of the triplets is a $J=3/2$ or $5/2$ 2D level. Thus if line polarization is detected in the 866nm line it cannot be due to scattering polarization. The angular momentum of the lower levels in all of these transitions allows for optical pumping. Thus, by detecting linear polarization in the reddest of the CaII near-IR triplet lines, we have clear evidence of OP absorptive polarization which cannot be caused by resonant scattering effects.

2.3. CaII NIR Triplet results

The CaII triplet lines in many of our stars are in emission, but of those systems with these lines in absorption, about half show complex Stokes Q,U polarization structure. Invariably the linear polarization morphology across the red triplet component is similar to the two bluer triplet components. An example is illustrated here. U Mon is an RVTau 91d variable star. Fig. 2 shows the intensity spectra and continuum normalized polarized spectra.

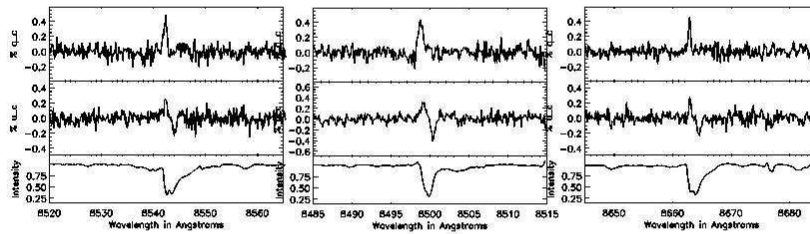


Figure 2. Spectra and continuum normalized Stokes Q and U spectra for U Mon in the CaII triplet lines

The Stokes Q and U polarized spectra show what we now know to be typical spectral line polarization variation, localized in the absorptive part of (in this case) the CaII triplet line cores. The linear polarization exhibits a typical amplitude of a few 0.1's of percent. The correspondence between the 866.2nm and the bluer triplet polarized spectra is clear evidence that it is an optical pumping mechanism which is responsible for the observed absorptive polarization signal.

2.4. Optical Pumping and Hyperfine Levels in Hydrogen

Hyperfine coupling of the atomic nuclear spin to the electronic levels implies that even $J=0$ ground-state levels may be sensitive to anisotropy in the radiation environment of a star. We've included this effect in hydrogen and built a radiation coupled model that includes 364 levels and about 5000 transitions up to $n = 6$ in hydrogen. Following (Kuhn et al. 2007) we've solved for the m -dependent equilibrium population in each of these levels as a function of the background radiation field anisotropy (parametrized by the radiation "cone-angle") and the radiation temperature. We assume that atomic collisions and magnetic field quantum coherence effects can be neglected. For the sufficiently intense radiation field and low density stellar environments that we consider here these are generally good assumptions. Thus Fig 3 shows that a 10,000K black-body with a 73deg illumination angle produces higher populations in the largest m -states at larger L . Note that the $n=1, L=0$ ground-state has opposite m -dependent anisotropy, that is, the $m=0$ populations are greater than higher magnitude m states. The relative population of higher n and L states is small but for more intense radiation (higher

temperature or larger illumination angle) the larger n and L states are relatively more heavily populated. As the cone angle (isotropy) increases the m -dependent population anisotropy decreases.

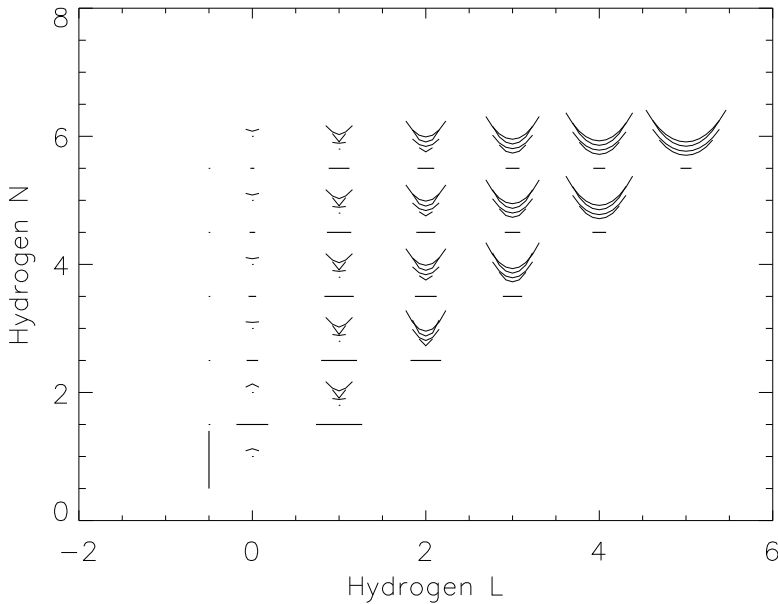


Figure 3. The relative population of hydrogen levels for a 10,000K black-body illuminating a collisionless gas with a 73deg cone angle. Hyperfine coupling is included and the curved lines show the relative population from $-m$ to $+m$ where m is the maximum magnetic total spin quantum number. The plot shows this population versus principal quantum number n and orbital angular momentum L . Thus for each n, L there are four levels with $F=L+1, 2 \times L$, and $L-1$. The thicker horizontal lines under each group of 4 total spin levels shows the relative population versus L for given n . The thick vertical lines are proportional to the relative population of all levels at given quantum number n . For example, here a 10000K black-body leaves most of the electrons in $n=1$ states. Only the $L=0,1$ states have significant population at larger n .

A strong m -dependent density dependence in radiation coupled levels in an atom can yield *opposite* population anisotropy in the upper and lower transition states. This is clear in Fig. 3 where the low lying $L=0$ states have higher $m=0$ populations, while the $L=1$ states have *lower* $m=0$ populations relative to higher magnitude magnetic quantum numbers. In this figure a positive or negative anisotropy is indicated by states with line curvature up versus down. A consequence of this is that as the radiative coupling changes because of a stronger radiation field (pumping region is closer to the star), or hotter radiation, the OP polarization changes rapidly. Thus, changing anisotropy (as radiation illumination cone angle changes) affects a competition between the opposite anisotropy composite states to produce significant net OP line polarization changes.

Polarization *ratios* of lines from the same term can be a very sensitive probe of the radiation strength and isotropy due to the opposite density anisotropy that is possible in low-lying atomic states. For example, we have computed the ratio of the theoretical

Balmer line polarization in H_β/H_α . Figure 4 plots the ratio of the $n=4$ to $n=2$ and the $n=3$ to $n=2$ transition polarizations versus the radiation illumination angle in degrees for a 10000K blackbody. The dotted curve shows that while the line intensity ratio is nearly constant as the radiation isotropy and strength vary, the polarization ratio even changes sign in a complex way. Line polarization ratios are a sensitive probe of the near stellar environment and contain radiation information distinct from the intensity line ratios.

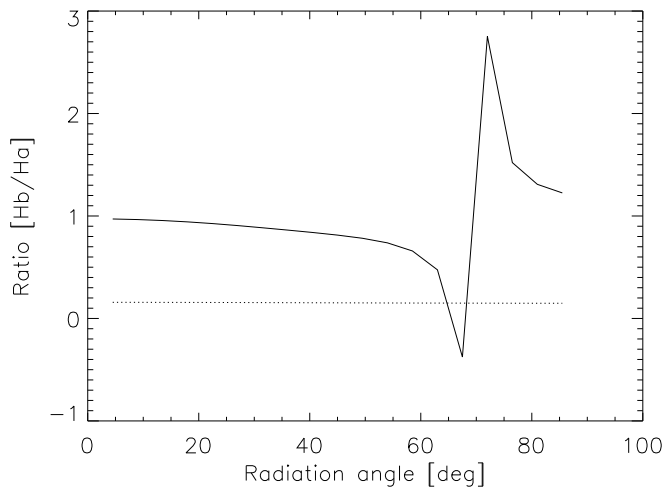


Figure 4. The solid line shows the ratio of H_β/H_α polarization and the dotted line shows the corresponding line intensity ratio versus radiation illumination cone angle. Competition between opposite density anisotropy low-lying hydrogenic levels causes a complicated polarization ratio as radiation coupling varies with cone angle.

Two examples illustrating a range of polarization and line ratios are SS Lep and MWC 361. SS Lep is a symbiotic binary star and MWC361 is a Herbig Be star with a directly detected disk (Okamoto et al. 2009). Figure 5 shows H_α and H_β for these two stars. The intensity ratio of the absorptive component of SS Lep and MWC 361 are about 0.3 and 0.2, while the corresponding polarization ratios are 0.3 and 0.1. Our work to uniquely interpret such line and polarization ratios is only beginning.

2.5. Geometric Properties from Absorptive Linear Spectropolarimetry

The mean radiation pumping direction at any point in the circumstellar cloud defines a direction projected onto the plane of the sky that, in the simplest approximation (see Fig. 1), is perpendicular to the mean electric field polarization of the transmitted light through the cloud at that location. If each location in the cloud encodes a definite doppler shift velocity, for example if the cloud is actually a rotating disk projected against the stellar disk, then the shape of the polarized absorptive line spectrum with wavelength gives information on the position angle of the disk in the sky and its inclination angle toward the observer.

Figure 6 shows an example of the expected Q, U polarization for a disk oriented as in the figure and observations from ϵ Aur that are consistent with this orientation. Sim-

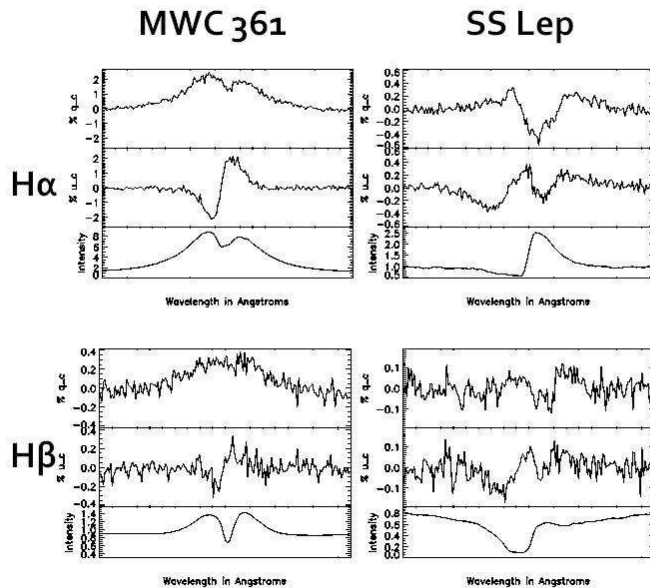


Figure 5. Each panel shows the Q, U, and I spectra near H_α and H_β for MWC 361 and SS Lep.

ilarly Figure 7 show the likely orientation of 51 Oph derived from H_α linear absorptive spectropolarimetry.

For a star with sufficient symmetry in its disk a straightforward procedure to derive the disk orientation is to plot the polarization angle at each wavelength across the absorptive line profile. Thus, in the case of MWC 361, if we derive an angle from $\theta = 1/2 \arctan(Q/U)$ and a polarization amplitude from $p = \sqrt{Q^2 + U^2}$ then a plot of $p(\theta)$ looks like Figure 8. The orientation of the disk is found by rotating the plot until symmetry about the x-axis is achieved. The data in Fig. 8 have been rotated about 5 degrees to yield symmetry around the x-axis suggesting that the position angle of the MWC 361 disk is 5 deg. This angle is consistent with the extended IR disk seen by Okamoto et al. (2009) but is at odds with the modeled rotation axis obtained from Zeeman Doppler Imaging (cf. Okamoto et al. 2009).

2.6. Absorptive Linear Polarization Imaging

With sufficient velocity resolution across the absorptive line profile the intensity and polarization amplitude and Q, U spectra may be inverted to yield the column density projected onto the star. Because the linear polarization is localized to the line-of-sight to the star, and analogous to the case of Doppler Zeeman Imaging for a stellar magnetic field, there is spatial information about the structure of the obscuring gas in front of the star in the Q, U spectra. In general the OP signal originates close to the pumping source – Kuhn et al. (2007) argued this is likely to be within 1 stellar radius of the photosphere. Either from the polarization amplitude or the absorbed intensity at each wavelength we

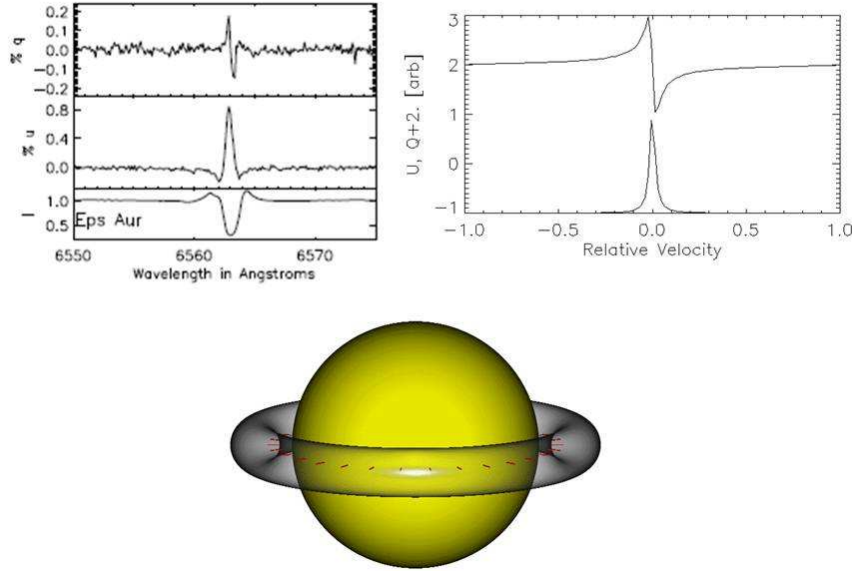


Figure 6. The observed Q and U spectra for ϵ Aur and a modeled linear polarization line profile for the indicated disk geometry. The small red lines in the disk are perpendicular to the transmitted light linear polarization direction at that projected disk location.

derive a local cloud “density” or optical depth. At each wavelength the Q, U polarization ratio defines an angle on the disk and the doppler velocity defines a surface (based on an assumed 3-space rotation profile or a wind velocity) the obscuring material must lie along. Alternatively the local polarization amplitude yields the separation between the local cloud position and the geometric center of the illuminating photosphere. We can demonstrate this using the H_α spectropolarimetry for AB Aur in order to obtain an “image” of the intervening cloud as shown in Figure 9. Here a radial outflow wind velocity was assumed and the inversion has a 180 degree ambiguity because of the linear polarization 2-fold rotational symmetry. The light shades in this figure indicate where the largest absorption against the stellar disk occurs as obtained from a single epoch inversion using high resolution I, Q, and U H_α spectra of AB Auriga.

3. Conclusions

Absorptive linear polarization is a nearly ubiquitous phenomenon in the spectra of imbedded stars. It is often visible in polarized Stokes Q and U spectra when a sensitivity better than 1% is achieved. We’ve shown that it is not a scattering phenomenon and is well described by optical pumping due to ground-state anisotropy from the anisotropic stellar radiation environment. We’ve shown here that there is new information on the stellar environment contained in linear spectropolarimetry that is distinct from, for ex-

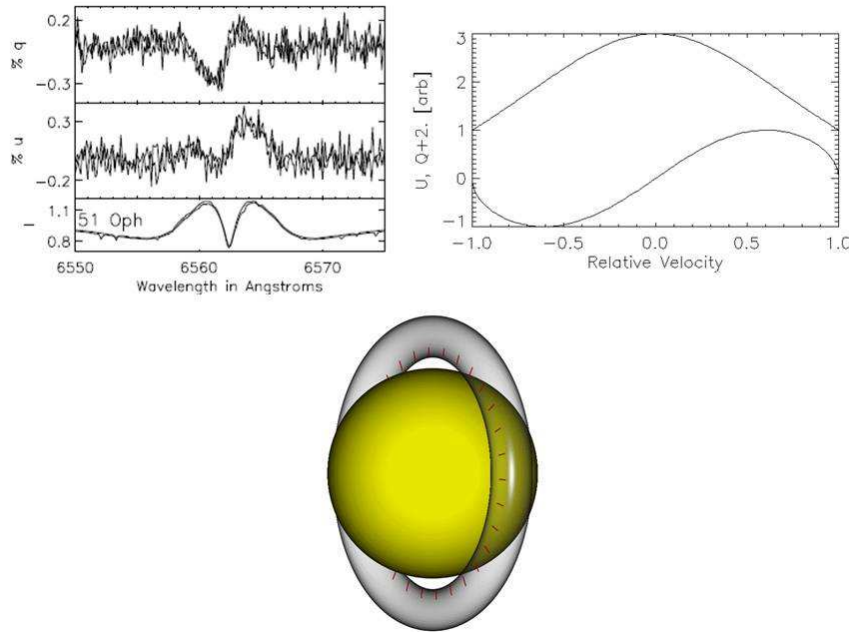


Figure 7. The observed Q and U spectra for the star 51 Oph and a correspondingly modeled linear polarization line profile for the indicated disk geometry. The small red lines in the disk/ring figure panel are perpendicular to the transmitted light linear polarization direction at that location.

ample, line intensity ratios. With simple assumptions, the geometry of stellar disks can be inferred. With additional assumptions we've demonstrated how high resolution spectropolarimetric data can be inverted to yield "images" of the intervening gas from polarized absorptive line profiles.

Acknowledgments. This research has been supported by the Institute for Astronomy on Maui. We're grateful to Svetlana Berdyugina who contributed to the hydrogenic hyperfine calculations.

References

- Happer, W. 1972, *Rev. Mod. Phys.* 44, 169
 Harrington D.M. & Kuhn J.R., *Spectropolarimetry of the H α line in Herbig Ae/Be stars*, 2007, *ApJL*, 667, L89
 Harrington D.M. & Kuhn J.R., *Spectropolarimetric observations of Herbig Ae/Be stars. I. HiVIS spectropolarimetric calibration and reduction techniques.*, 2008, *PASP*, 120, 89
 Harrington D.M. & Kuhn J.R., *Spectropolarimetric observations of Herbig Ae/Be stars. II. Comparison of spectropolarimetric surveys: Herbig Ae/Be, Be and other emission-line systems.*, 2009a, *ApJS*, 180, 138
 Harrington, D. M. & Kuhn J.R., *Ubiquitous H α -Polarized Line Profiles: Absorptive Spectropolarimetric Effects*, 2009b, *ApJ*, 695, 238

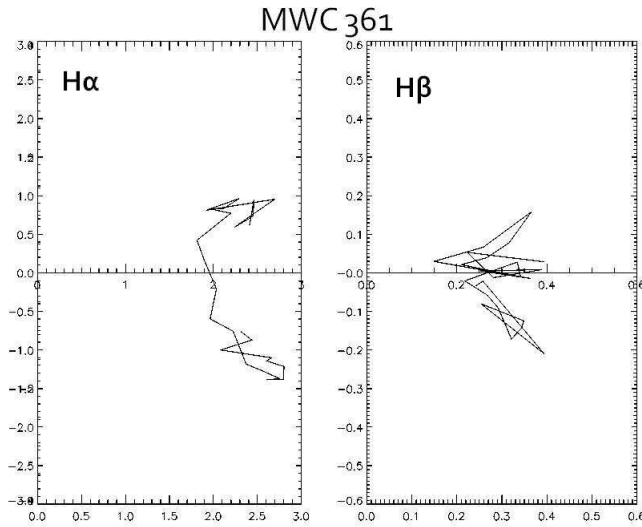


Figure 8. The H_α and H_β Q, U amplitude and direction are plotted as a collection of points across the absorptive line profile. Rotating these points to a symmetry line around the x-axis shows that the disk position angle is about 5 degree in the sky.

- Kuhn J.R., Berdyugina S.V., Fluri D.M., Harrington D.M. & Stenflo J.O., *A new mechanism for polarizing light from obscured stars*, 2007, *ApJL*, 668, L63
- Manso Sainz, R., & Trujillo Bueno, J. *Zero Field Dichroism in the Solar Chromosphere*, 2003, *PRL*, 91, 111102
- McLean I.S., *Interpretation of the intrinsic polarizations of early-type emission-line stars*, 1979, *MNRAS*, 186, 265
- Okamoto, Y. K. et al. *Direct Detection of a flared disk around a young massive star*, 2009, *ApJ* 706, 665
- Oudmaijer R.D., & Drew J.E., *H α spectropolarimetry of B[e] and Herbig Be stars*, 1999, *MNRAS*, 305, 166
- Trujillo Bueno, J., Landi Degl'Innocenti, E. 1997 *ApJ* 482, L183
- Vink J.S., Drew, J.E., Harries T.J., and Oudmaijer R.D., *Probing the circumstellar structure of Herbig Ae/Be stars*, 2002, *MNRAS*, 337, 356
- Vink, J.S., Harries T.J., and Drew J.E., *Polarimetric line profiles for scattering off rotating disks*, 2005, *A&A*, 430, 213
- Vink J.S., Drew J.E., Harries T.J., Oudmaijer R.D., and Unruh Y., *Probing the circumstellar structures of T Tauri stars and their relationship to those of Herbig stars*, 2005, *MNRAS*, 359, 1049

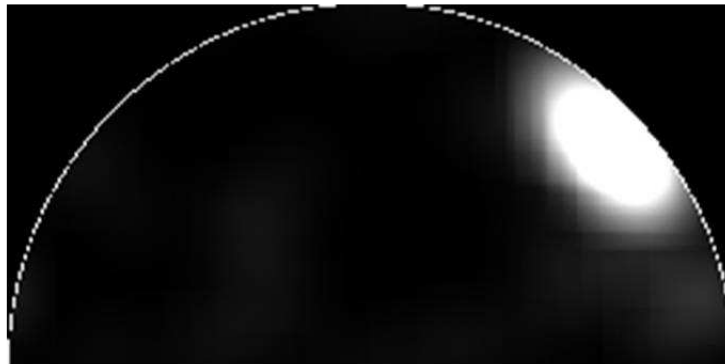
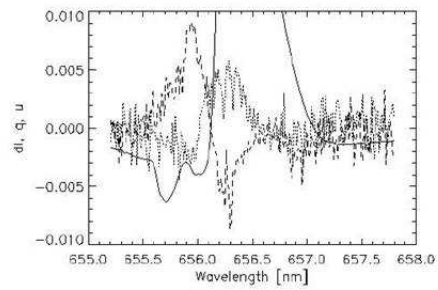


Figure 9. From the high resolution I, Q, and U spectra of H_α we derive the projected optical depth of intervening hydrogen gas in the side panel of this figure. Lighter shades indicate higher depth.